Supporting Information

Plasma extracellular vesicle phenotyping for the differentiation of early-stage lung cancer and benign lung disease

Liwen Yuan[1,†], Yanpin Chen[2,†], Longfeng Ke[3], Quan Zhou[4], Jiayou Chen[5], Min Fan[1], Alain Wuethrich[4*], Matt Trau[4,6*], Jing Wang[1*]

[1]Key Laboratory of OptoElectronic Science and Technology for Medicine of Ministry of Education, Fujian Provincial Key Laboratory of Photonics Technology, Fujian Normal University, Fuzhou 350117, China

[2]Department of Pathology, Clinical Oncology School of Fujian Medical University and Fujian Cancer Hospital, Fuzhou, Fujian 350014, China

[3]Laboratory of Molecular Pathology, Clinical Oncology School of Fujian Medical University and Fujian Cancer Hospital, Fuzhou, Fujian 350014, China

[4]Centre for Personalized Nanomedicine, Australian Institute for Bioengineering and Nanotechnology (AIBN), The University of Queensland, Brisbane, QLD 4072, Australia

[5]Department of Radiology, Clinical Oncology School of Fujian Medical University and Fujian Cancer Hospital, Fuzhou, Fujian 350014, China

[6]School of Chemistry and Molecular Biosciences, The University of Queensland, Brisbane, QLD 4072, Australia

*Corresponding authors: a.wuethrich@uq.edu.au; m.trau@uq.edu.au; jing.wang@fjnu.edu.cn

†Equal Contribution

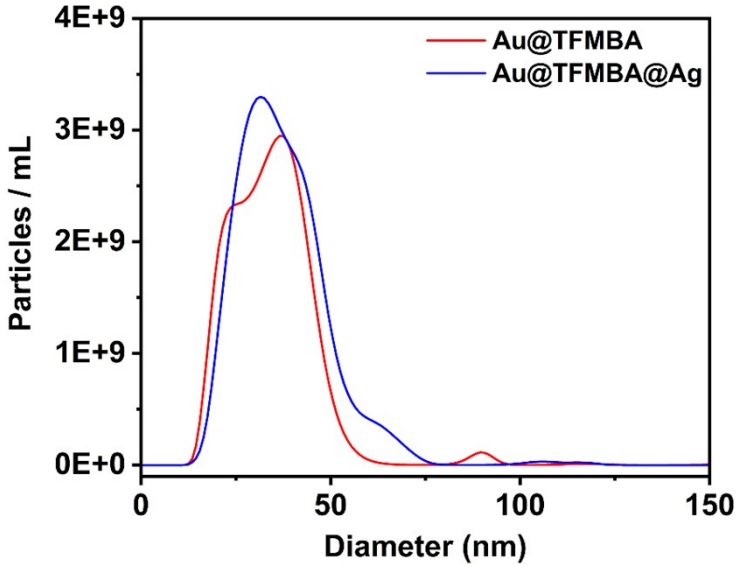

Figure S1. The size distributions of Au@TFMBA and Au@TFMBA@Ag NPs measured by the nanoparticle tracking analysis.

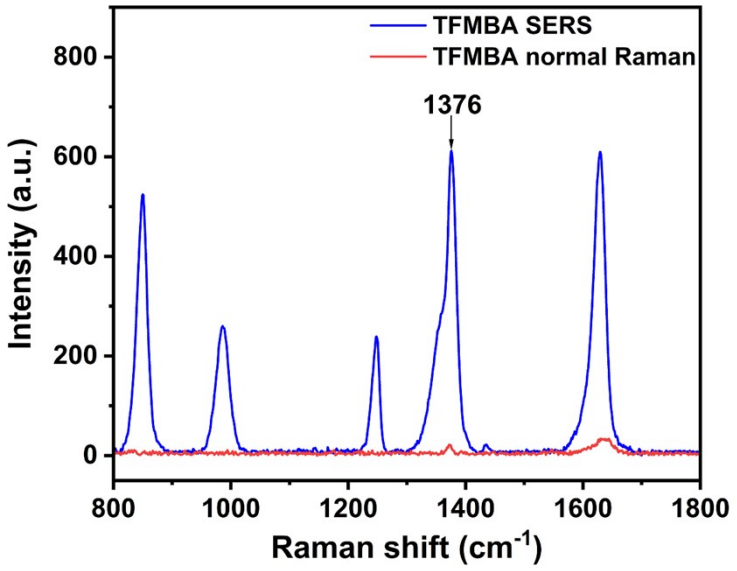

Figure S2. Comparison of Raman signals of Au@TFMBA@Ag NPs with 20 mM TFMBA molecules in water.

SERS enhancement factor

Au@TFMBA@Ag NPs were used as an example to determine the enhancement factor of Au@Ra@Ag NPs. The enhancement factor was calculated using the equation (1):

$$EF = {I_{SERS} \times C_{Raman}}/{I_{Raman}} \times C_{SERS} \quad (1)$$

where C_{Raman} and C_{SERS} refer to the concentrations of TFMBA in Raman and SERS measurements; I_{SERS} and I_{Raman} represent SERS and Raman intensities of TFMBA at 1376 cm^{-1}.

Both SERS nanotags and TFMBA molecules (20 mM) were resuspended in water in a cuvette for measurements. The spectral signal was detected using a portable IM-52 Raman Microscope. Samples were excited by the 785-nm laser wavelength for 1-s integration time. The resulting spectra of SERS nanotags and TFMBA molecules were indicated in Fig. S4, showing intensities of 612 a.u. and 15 a.u., respectively.

Nanoparticle tracking analysis was used for measuring the concentration ($C_{nanotag}$) and the average diameter of SERS nanotag ($D_{nanotag}$), which were $9.04\times10^{10} \pm 1.02\times10^{10}$ particles/mL and 37.4 nm ± 0.1 nm, respectively. C_{SERS} was calculated using the equation (2):

$$C_{SERS} = {C_{nanotag} \times S_{nanotag}}/{S_{TFMBA}} = {C_{nanotag} \times \pi D_{nanotag}^{2}}/{S_{TFMBA}} \quad (2)$$

Where $S_{nanotag}$ and S_{TFMBA} respectively refer to the surface area of SERS nanotags and topological polar surface area of TFMBA (0.383 nm^2)[1]. Accordingly, the C_{SERS} and EF were calculated to be 1.02×10^{15} molecules/mL and 4.74×10^{5}, respectively.

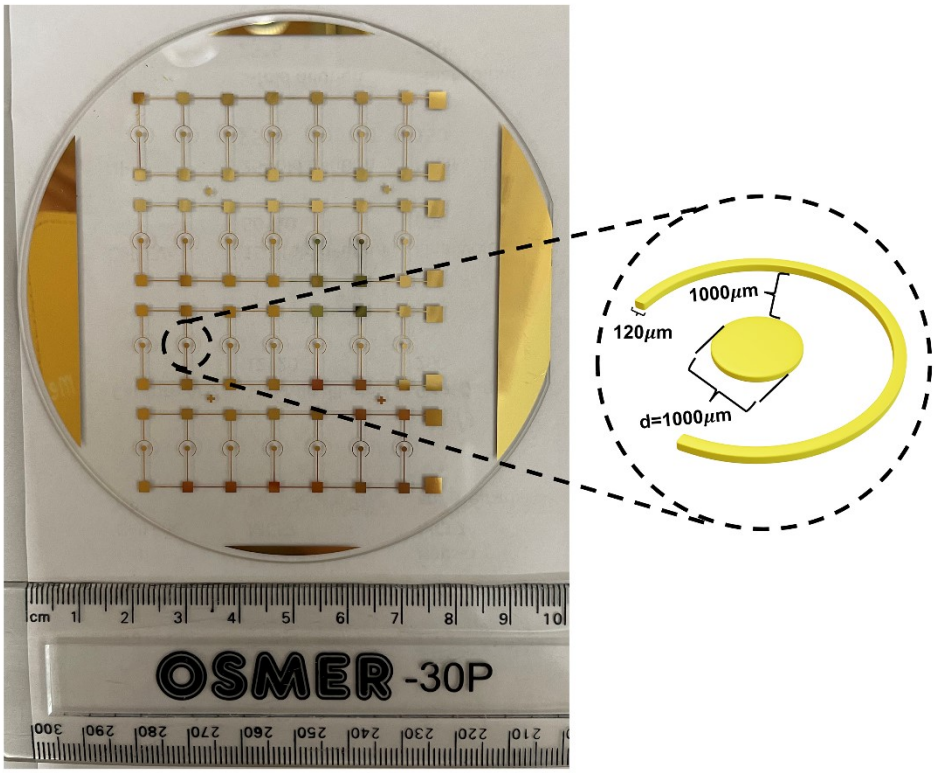

Figure S3. The design of the nanomixing chip. The nanomixing chip was arrayed with multiple pairs of asymmetric gold electrodes consisting of inner circular electrodes (diameter=1000 μm) and outer ring electrodes (width=120 μm), which were separated by 1000 μm.

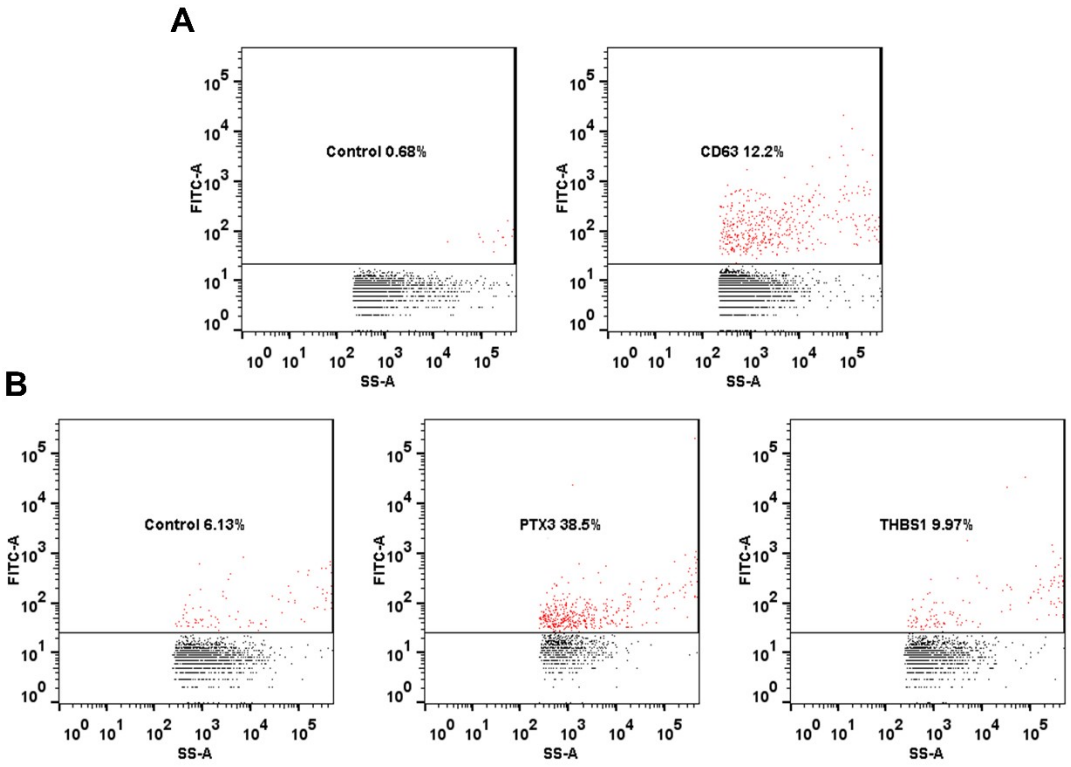

Figure S4. Nanoflow cytometry characterization of A549-derived EV surface proteomics. The expression of (A) CD63, (B) PTX3 and THBS1 on A549-derived EV surfaces. The characterization of CD63, PTX3 and THBS1 expression on EV surfaces was performed individually. The controls in nanoflow cytometry characterization of (A) CD63 and (B) PTX3 and THBS1 on EV surfaces are different, including (A) EVs with FITC-conjugated IgG antibodies and (B) EVs with FITC-conjugated anti-IgG antibodies.

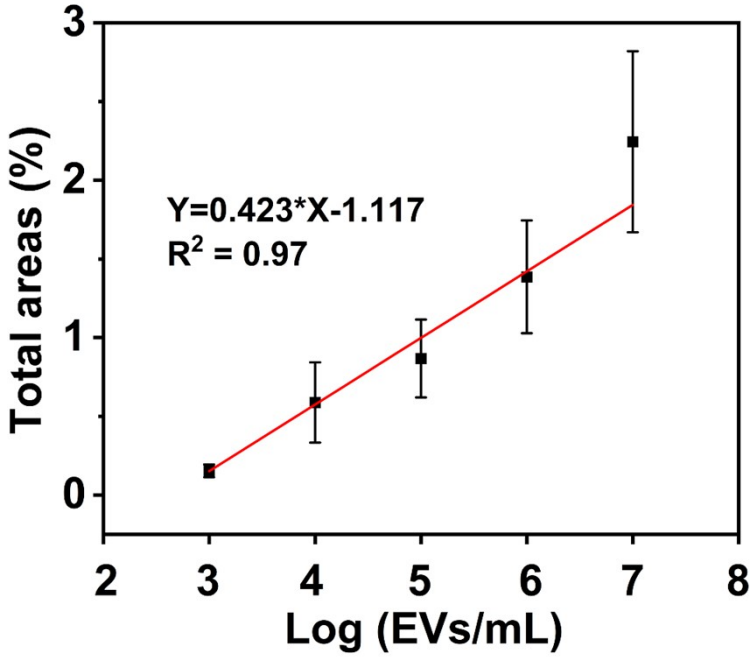

Figure S5. The total percentages of signal dot areas to mapping areas-EV concentration response curve. Data are represented as mean ± standard deviation, where error bars represent the standard deviation of three independent experiments (n=3).

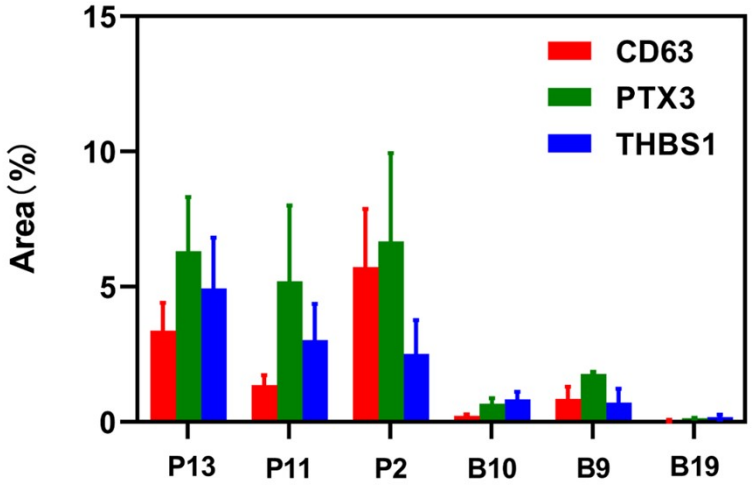

Figure S6. The SERS signatures of representative early-stage lung cancer patients (P13, P11, and P2) and patients with benign lung diseases (B10, B9 and B19). Data are represented as mean ± standard deviation, where error bars represent the standard deviation of three independent experiments (n=3).

Table S1. The demographic data, CT nodule classification, and pathological results for individual lung cancer patients, patients with benign lung diseases, and healthy controls.

Patient ID	Gender	Age	Nodule classification	Stage	Pathology
P1	M	65	Solid	IA 3	IAC
P2	M	48	Mixed GGN	IA 2	MIA
P3	F	62	Solid	IA 2	MIA
P4	M	70	Solid	IA 2	MIA
P5	F	54	Mixed GGN	IA 2	MIA
P6	F	61	Pure GGN	0	AIS
P7	M	40	Solid	0	AIS
P8	F	49	Solid	IB	IAC
P9	F	68	Mixed GGN	IA 2	MIA
P10	M	65	Unknown	IA 3	IAC
P11	F	63	Pure GGN	IA	AIS
P12	F	63	Mixed GGN	IA 2	IAC
P13	M	79	Solid	IA 2	IAC
P14	F	60	Mixed GGN	IA 2	IAC
P15	M	61	Solid	IB	IAC
P16	F	64	Solid	IA 1	IAC
P17	F	60	Pure GGN	IA 1	AIS
P18	F	57	Mixed GGN	IA 1	MIA
P19	M	62	Mixed GGN	IA 1	MIA
P20	F	82	Mixed GGN	IA 2	IAC
P21	M	49	Mixed GGN	IA 2	IAC
P22	M	54	Pure GGN	IA 2	IAC
P23	M	46	Mixed GGN	IA 1	MIA
P24	M	60	Solid	IA 2	IAC

P25	F	62	Solid	IA 1	IAC
P26	F	66	Mixed GGN	0	MIA
P27	F	45	Unknown	0	AIS
P28	F	30	Solid	IA 1	IAC
B1	M	68	Solid		
B2	M	75	Mixed GGN		
B3	F	45	Solid		
B4	F	57	Solid		
B5	M	53	Solid		
B6	F	56	Solid		
B7	F	58	Solid		
B8	M	65	Solid		
B9	M	53	Pure GGN		
B10	F	41	Solid		
B11	F	68	Solid		
B12	M	60	Solid		N/A
B13	F	50	Solid		
B14	M	50	Solid		
B15	M	48	Unknown		
B16	M	64	Solid		
B17	M	72	Solid		
B18	F	50	Solid		
B19	F	52	Mixed GGN		
B20	M	76	Solid		
B21	M	52	Solid		
B22	M	36	Solid		
B23	M	56	Solid		
H1	M	29		N/A	

H2	M	22
H3	F	24
H4	M	20
H5	M	28
H6	F	25
H7	M	23
H8	M	29
H9	F	38
H10	M	47
H11	F	24
H12	F	26
H13	F	25
H14	M	31
H15	F	24
H16	M	32
H17	M	24
H18	M	26
H19	F	24
H20	M	41
H21	M	46
H22	M	20
H23	M	31
H24	F	30
H25	F	26
H26	F	29

Abbreviations: ground-glass nodule, GGN; adenocarcinoma in situ, AIS; minimally invasive adenocarcinoma, MIA; invasive adenocarcinoma, IAC.

Reference

1. Y. Liu, N. Lyu, V. K. Rajendran, J. Piper, A. Rodger and Y. Wang, *Anal. Chem.*,

2020, **92**, 5708-5716.